THE JOURNAL OF BIOLOGICAL CHEMISTRY VOL. 290, NO. 20, pp. 12765–12778, May 15, 2015

Heterotrimeric Kinesin-2 (KIF3) Mediates Transition Zone and Axoneme Formation of Mouse Photoreceptors*

Received for publication, January 14, 2015, and in revised form, March 29, 2015 Published, JBC Papers in Press, March 30, 2015, DOI 10.1074/jbc.M115.638437

Li Jiang[‡1], Yuxiao Wei[‡], Cecinio C. Ronquillo[‡], Robert E. Marc[‡], Bradley K. Yoder[§], Jeanne M. Frederick[‡], and Wolfgang Baehr[‡¶‖2]

From the Departments of [‡]Ophthalmology and Visual Sciences and [‖]Neurobiology and Anatomy, University of Utah Health Science Center, Salt Lake City, Utah 84132, the [§]Department of Cell, Developmental and Integrative Biology, University of Alabama at Birmingham, Birmingham, Alabama 35294, and the [¶]Department of Biology, University of Utah, Salt Lake City, Utah 84112

Background: Heterotrimeric kinesin-2 (KIF3) has been implicated in intraflagellar trafficking of photoreceptor membrane proteins by IFT.
Results: KIF3 and IFT88 are required for transition zone and axoneme formation, but are dispensable for rhodopsin trafficking.
Conclusion: Transmembrane proteins, including rhodopsin, traffic to the OS even when IFT is disabled.
Significance: KIF3 builds and maintains the photoreceptor transition zone and axoneme that are essential for photoreceptor integrity and vision.

Anterograde intraflagellar transport (IFT) employing kinesin-2 molecular motors has been implicated in trafficking of photoreceptor outer segment proteins. We generated embryonic retina-specific (prefix "emb") and adult tamoxifen-induced (prefix "tam") deletions of KIF3a and IFT88 in adult mice to study photoreceptor ciliogenesis and protein trafficking. In $^{emb}Kif3a^{-/-}$ and in $^{emb}Ift88^{-/-}$ mice, basal bodies failed to extend transition zones (connecting cilia) with outer segments, and visual pigments mistrafficked. In contrast, $^{tam}Kif3a^{-/-}$ and $^{tam}Ift88^{-/-}$ photoreceptor axonemes disintegrated slowly post-induction, starting distally, but rhodopsin and cone pigments trafficked normally for more than 2 weeks, a time interval during which the outer segment is completely renewed. The results demonstrate that visual pigments transport to the retinal outer segment despite removal of KIF3 and IFT88, and KIF3-mediated anterograde IFT is responsible for photoreceptor transition zone and axoneme formation.

Primary cilia are axoneme-stabilized protrusions that elongate from the basal body (mother centriole) of most vertebrate cell types (1–3). Cilia serve as a cell's "antenna" to sample a broad range of extracellular signals in olfaction, vision, taste, and mechanosensation (4, 5). Primary cilia of kidney epithelia are mechanosensitive, detecting fluid flow through the tubule (6). Cilia of olfactory epithelia distinguish a large number of odorants (7). Photoreceptor sensory cilia detect light of different wavelengths and are responsible for dim light and color vision (8). The photoreceptor sensory cilium is composed of the outer segment (OS)[3] containing a stack of disc membranes, a basal body (microtubule-organizing center), and an axoneme. Each OS communicates with its inner segment (IS) through a connecting cilium, a structure equivalent to the transition zone of primary cilia (9). In the following, the term "connecting cilium" will be replaced by "photoreceptor transition zone" or PTZ.

Intraflagellar transport (IFT) is a bidirectional ciliary trafficking pathway conserved between invertebrates and vertebrates (5). Protein complexes and IFT particles (IFT-A and IFT-B) traffic along the flagellar/ciliary axoneme, a pathway integral for assembly, maintenance, and function of motile and primary cilia (10–12). IFT defects cause human syndromic and nonsyndromic ciliopathies, a group of diseases affecting the function of sensory cilia and survival of entire organs (13). The IFT-B particle IFT88 (Tg737 or Polaris), located at basal bodies and axonemes, is required for anterograde trafficking and ciliary assembly (10, 14). *Chlamydomonas* mutants lacking IFT88 are viable but do not form flagella (14), and zebrafish *Ift88* mutants never develop photoreceptor outer segments (15). Germline deletions of IFT88 are embryonically lethal (14, 16), and hypomorphic mutations ($Tg737^{orpk}$ mice) cause complex ciliopathies affecting multiple tissues including photoreceptors, kidney, and olfactory neurons (17–20). IFT88 was shown by pulldowns to be associated with rhodopsin, GC1, and a chaperone termed mammalian relative of Dna-J (MRJ) suggesting that outer segment transmembrane proteins are IFT cargo (21). However, the precise composition of IFT cargo is unknown.

Heterotrimeric kinesin-2 (KIF3, consisting of KIF3A, KIF3B, and kinesin-2-associated protein (KAP) subunits) (22) is a canonical plus-oriented anterograde IFT motor. Discovered in sea urchin eggs (23), KIF3 is present in a broad range of species, including *Chlamydomonas* (24, 25), *Caenorhabditis elegans* (26), and zebrafish (10, 27, 28). Germline deletion of mouse KIF3a is embryonically lethal, and photoreceptor-specific dis-

* This work was supported by National Institutes of Health Grants EY08123, EY019298 (to W. B.), and EY014800-039003 (NEI core grant) to the Department of Ophthalmology, University of Utah, a Research to Prevent Blindness (RPB) Nelson Trust Award (to W. B.), and unrestricted grants to the Departments of Ophthalmology at the University of Utah from RPB.
[1] To whom correspondence may be addressed. E-mail: li.jiang@hsc.utah.edu.
[2] The recipient of a Research to Prevent Blindness Senior Investigator Award. To whom correspondence may be addressed. E-mail: wbaehr@hsc.utah.edu.
[3] The abbreviations used are: OS, outer segment; IS, inner segment; IFT, intraflagellar transport; PTZ, photoreceptor transition zone; ONL, outer nuclear layer; COS, cone outer segment; ROS, retinal outer segment; ERG, electroretinography; PTI, post-tamoxifen induction; CNG, cyclic nucleotide-gated; ORPK, Oak Ridge Polycystic Kidney; emb, embryonic retina-specific; tam, adult tamoxifen-induced; cd, candelas; P, postnatal day.

ruption of KIF3A caused OS protein mistrafficking with rapid degeneration (29, 30). Conditional KIF3A knockouts, studied in several organs and including renal tubules, resulted in ciliary loss (31). A conditional KIF3A knock-out in mouse cones prevented trafficking of opsins and other phototransduction components (32). However, mouse rods deficient in KIF3A showed normal trafficking of phototransduction components even as rods underwent rapid degeneration (32), suggesting redundancy of rod anterograde IFT motor(s) or motor-independent trafficking pathways (33–35).

This study addresses KIF3 and IFT88 in mouse photoreceptor ciliogenesis, IFT, and rhodopsin trafficking. We used a two-tiered conditional approach to determine whether time of deletion affected the photoreceptor phenotype, *i.e.* deletion of each KIF3A and IFT88 in photoreceptor progenitors and depletion in adult photoreceptors by tamoxifen induction. Retina-specific deletion of either KIF3A or IFT88 during early development resulted in failure to form PTZs; depletion of either KIF3A or IFT88 by tamoxifen induction resulted in progressive, distal shortening of the OS axoneme, despite continued rhodopsin trafficking for at least 10 days. Our data indicate that the phenotype of KIF3 loss strongly depends on the time of *Cre*-driven recombination, and that KIF3-driven IFT functions primarily in photoreceptor ciliogenesis, PTZ formation, and axoneme stabilization.

EXPERIMENTAL PROCEDURES

Mice—*Kif3a*$^{flox/flox}$ and *Ift88*$^{flox/flox}$ mice (29, 36) were used to generate *Kif3a* and *Ift88* conditional knock-out mice. Several *Cre* mouse strains, *Six3Cre*, *CreER* (The Jackson Laboratory stock number 004682), *EIIaCre* (The Jackson Laboratory stock number 003724), and *iCre75*, were used to disrupt conditionally the *Kif3a* and *Ift88* genes (32, 37–40). *Rho*$^{-/-}$ mice (41) and transgenic mice expressing S-opsin protein in rod photoreceptors (42) were obtained from Janis Lem (Tufts University) and Jason Chen (Baylor College of Medicine), respectively. A transgenic mouse expressing GFP-CETN2 fusion protein (The Jackson Laboratory stock number 008234) permits observation of centrioles and photoreceptor-connecting cilia with fluorescence microscopy (43). To induce *Cre* activity in *CreER* mouse, tamoxifen (150 mg/kg of body weight) was injected intraperitoneally at 1–2 months of age for 5 consecutive days. Tamoxifen stock solution (20 mg/ml) was prepared by dissolving tamoxifen powder in corn oil (each from Sigma-Aldrich). The Institutional Animal Care and Use Committee (IACUC) of the University of Utah, in compliance with statements for animal use of the Association for Research in Vision and Ophthalmology (ARVO), approved all experiments. Mice were maintained under 12-h cyclic dark/light conditions.

Antibodies—Rabbit anti-KIF3A (K3513; Sigma-Aldrich), rabbit anti-KIF17 (ab11261; Abcam, Cambridge, MA), and goat anti-IFT88 (kindly provided by J. Besharse, Medical College of Wisconsin, Milwaukee, WI) antibodies were used to detect IFT motors, kinesin-2, and IFT88 polypeptides. Antibodies directed against photoreceptor OS proteins and synaptic terminal proteins were previously described (32, 44). Mouse anti-Ac-tubulin (T6793; Sigma-Aldrich) and chicken anti-RP1 (kindly provided by Eric Pierce, Harvard Medical School) antibodies were used to detect the microtubule-containing axonemes.

Western Blot—Mouse retinas were lysed by sonication in radioimmuneprecipitation assay buffer (150 mM NaCl, 1% NP-40, 0.5% sodium deoxycholate, 1% SDS, 50 mM Tris-HCl, pH 8.0). The supernatant of each lysate was separated by 10% SDS-PAGE (~15 μg of protein/well), and then transferred to a nitrocellulose membrane (Bio-Rad). The membrane was probed subsequently with primary antibodies, followed by HRP-conjugated secondary antibody. Phosphorescence (ECL system, PerkinElmer) was used to visualize the signal on x-ray film.

Immunohistochemistry—Mouse eyeballs were isolated and immediately immersion-fixed with 4% paraformaldehyde in 0.1 M phosphate buffer, pH 7.4, for 2 h on ice (45). After removal of the anterior segment, each eyecup was equilibrated sequentially with 15 and 30% sucrose in 0.1 M phosphate buffer for cryoprotection. The eyecups were then embedded in OCT and cut into 12-μm-thick retina sections. The sections were incubated in each primary antibody at 4 °C overnight after blocking with 10% donkey serum and washed three times with phosphate buffer. Sections were then incubated in fluorescent-conjugated secondary antibodies at room temperature for 1–2 h, washed three times, and mounted with VECTASHIELD medium (Vector Laboratories, Burlingame, CA). DAPI (1:50000, Invitrogen) was added to the secondary antibody solution to distinguish nuclei. Images were captured using an Olympus FluoView 1000 confocal microscope with either 60× and/or 100× objective lenses.

Electron Microscopy—Isolated mouse eyecups were fixed by immersion in fixative solution (2% glutaraldehyde, 1% paraformaldehyde in 0.1 M cacodylate buffer, pH 7.4) at 4 °C overnight (32, 46). The eyecups were then postfixed with 1% osmium tetroxide in 0.1 M cacodylate for 1 h, buffer-rinsed, stained *en bloc* with uranyl acetate, and subsequently dehydrated in an ascending series of methanol solutions. Eyecups were embedded in Epon resin (Ted Pella, Inc., Redding, CA) for sectioning. 1-μm sections were cut to orient photoreceptors near the optic nerve. Retina ultrathin (60-nm) sections were cut onto slot grids with carbon-coated Formvar film (Electron Microscopy Sciences, Hatfield, PA) and post-stained with uranyl acetate followed by lead citrate. Transmission electron microscopy was performed at 75 kV using a JOEL electron microscope.

Electroretinography (ERG)—Full-field ERGs were performed on *Kif3a* mutant and control mice using a UTAS E-3000 system (LKC Technologies, Inc.; Gaithersburg, MD) as described (45). Briefly, dark-adapted mice were anesthetized by intraperitoneal injection with 10 mg/ml ketamine, 1 mg/ml xylazine (10 μl/g of body weight), and pupils were dilated by applying a drop of 2.5% phenylephrine (Akorn, Inc., Decatur, IL). For scotopic ERG, mice were stimulated by flashes with different intensities ranging from −40 db (−3.4 log cd m^{-2}) to 25 db (2.9 log cd m^{-2}) without initial rod saturation, and their retinal responses were recorded. To record photopic ERG responses, a rod-saturating background light of 10 db (1.48 log cd m^{-2}) was applied for 20 min before and during recording. Single-flash responses were usually recorded at stimulus intensities of −10 db (−0.6 log cd m^{-2}) to 25 db (2.9 log cd m^{-2}). Five or fewer flashes were averaged per intensity level with longer flash intervals with increasing intensity. 3–5 mice were tested for each group.

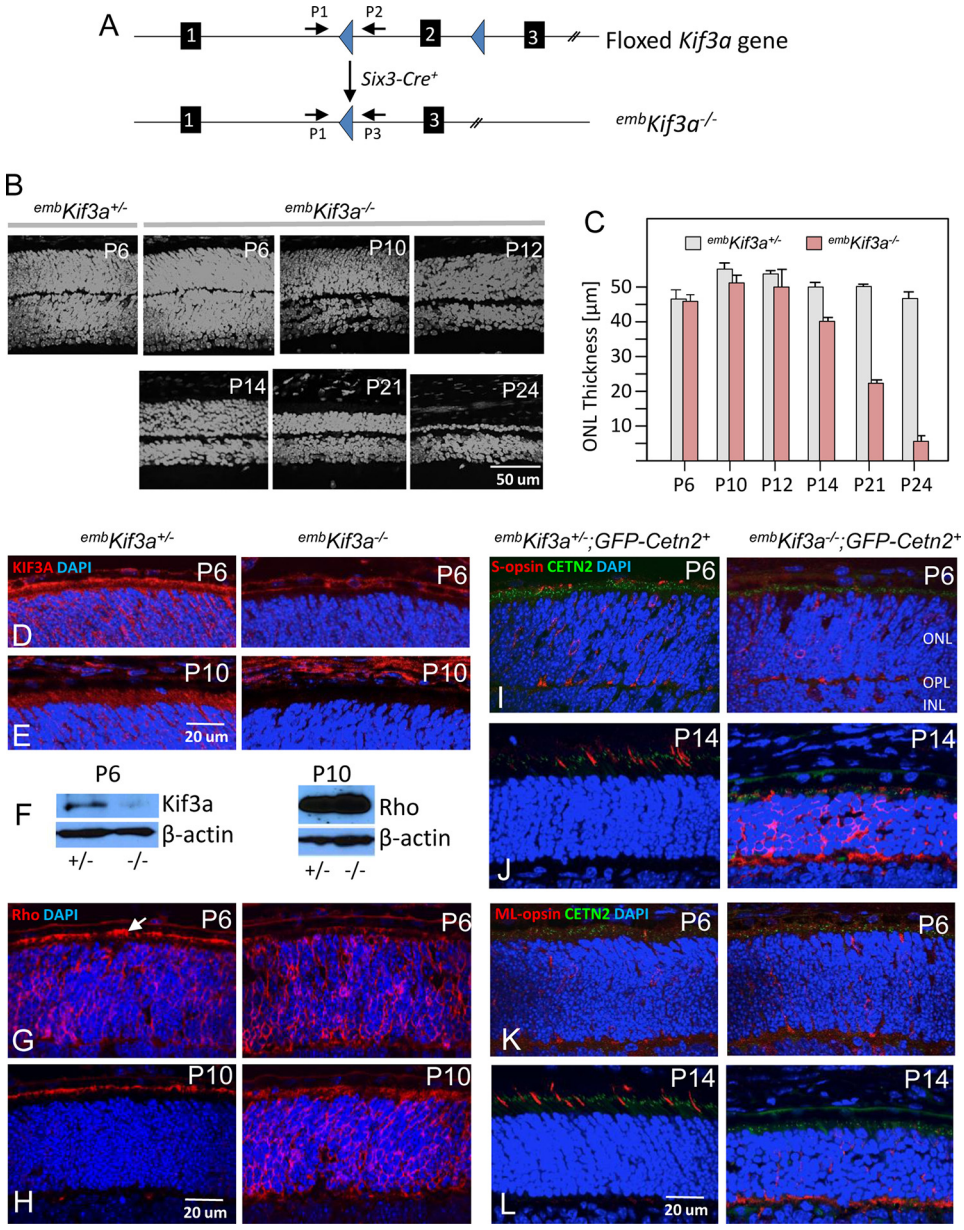

FIGURE 1. **Rapid photoreceptor degeneration in $^{emb}Kif3a^{-/-}$ mice.** *A*, generation of embryonic retina-specific *Kif3a* knockouts ($^{emb}Kif3a^{-/-}$). $Kif3a^{flox/flox}$ mice are mated with transgenic mice expressing *Cre* recombinase under control of a *Six3* promoter. *Top*, floxed gene with loxP sites in introns 1 and 2. *Bottom*, targeted gene with deletion of exon 2. Primers 1–3 are used for genotyping *Kif3a* alleles (29, 32). *B*, representative retina transverse sections at various postnatal times (P6–P24, as indicated). Onset of ONL degeneration is first apparent in the P14 knock-out. The ONL continues to shrink at P14 and P21, with only a single nuclear row present at P24. *C*, quantitation of ONL thickness (in μm) of heterozygous and homozygous knockouts. *D* and *E*, immunohistochemistry of $^{emb}Kif3a^{+/-}$ (*left*) and $^{emb}Kif3a^{-/-}$ (*right*) retina cryosections probed with anti-KIF3A (*red*) antibody at P6 (*D*) and P10 (*E*). DAPI (*blue*) labels nuclei. *F*, immunoblot of $^{emb}Kif3a^{+/-}$ and $^{emb}Kif3a^{-/-}$ P6 retina lysate with anti-KIF3A antibody (*left*) and of P10 retina lysate with anti-rhodopsin antibody (*right*). β-Actin was used as immunoblot loading control. *G* and *H*, rhodopsin localization in $^{emb}Kif3a^{+/-}$ (*left*) and $^{emb}Kif3a^{-/-}$ (*right*) retina sections at P6 (*G*) and P10 (*H*), respectively. *I–L*, localizations of S-opsin (*I* and *J*) and ML-opsin (*K* and *L*) in $^{emb}Kif3a^{+/-}$;$Cetn2^{+}$ and $^{emb}Kif3a^{-/-}$;$Cetn2^{+}$ retina. GFP-CENT2 (*green*) is a connecting cilium/centriole marker. *OPL*, outer plexiform layer; *INL*, inner nuclear layer.

Data Analysis—Retina degeneration was evaluated by measurement of the outer nuclear layer (ONL) thickness in μm ($n = 3$) with standard deviation. About 100–150 photoreceptors were examined for PTZ formation of each type, and the results were presented as percentages of cells with and without PTZ. Photoreceptor axoneme length was measured in ImageJ (50 photoreceptors each type) and analyzed with *t* test. ERG data ($n = 3$) was analyzed by two-way analysis of variance.

RESULTS

Early Loss of KIF3A Causes Rapid Photoreceptor Degeneration and Membrane Protein Mislocalization—We deleted KIF3A conditionally in photoreceptor progenitors by mating *Kif3a* floxed mice (29, 32) with Six3Cre mice (37) to generate $Kif3a^{f/f}$;$Six3Cre^{+}$ ($^{emb}Kif3a^{-/-}$) (Fig. 1*A*). Under control of the Six3 promoter, *Cre* is expressed in mouse neuroretina progenitors as early as embryonic day 9.5 (37); therefore KIF3A is expected to be deleted before photoreceptor differentiation in

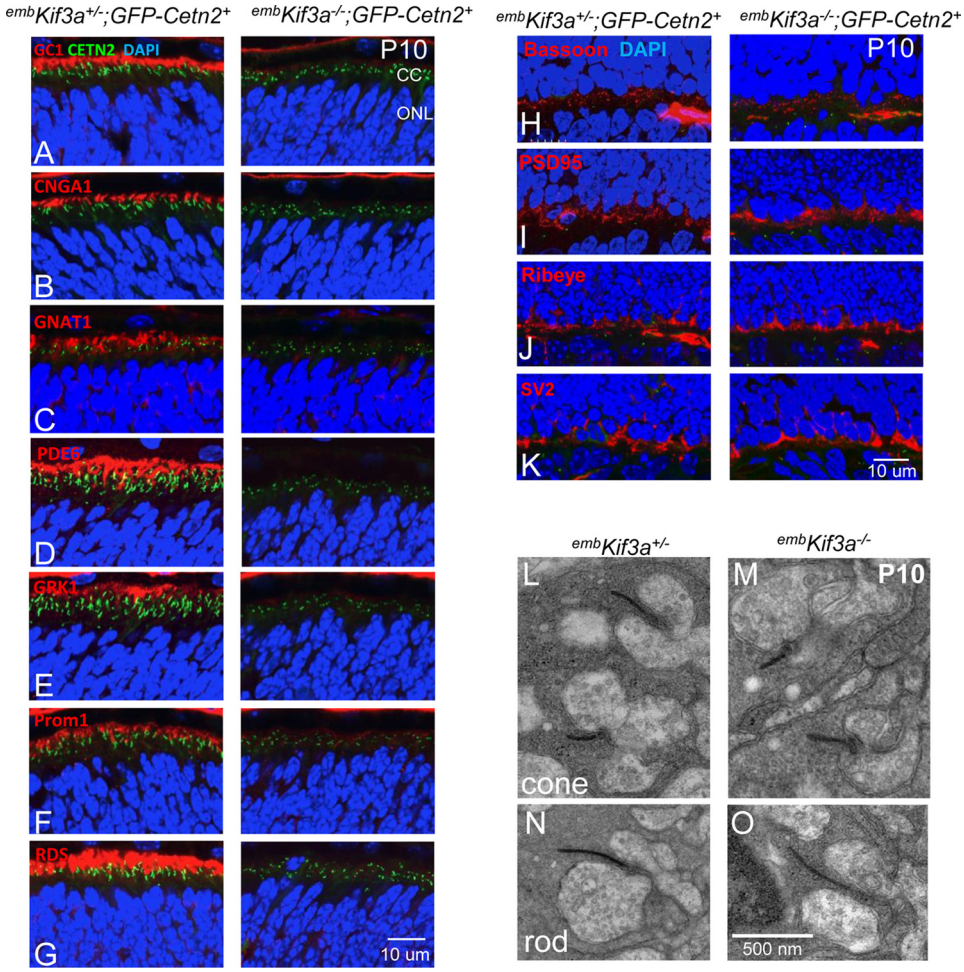

FIGURE 2. **Failure of OS protein trafficking in $^{emb}Kif3a^{-/-}$;$Cetn2^{+}$ photoreceptors.** *A–G*, $^{emb}Kif3a^{+/-}$;$Cetn2^{+}$ (*left*) and $^{emb}Kif3a^{-/-}$;$Cetn2^{+}$ (*right*) retina sections probed with: anti-GC1 (GUCY2E) (*A*); anti-cyclic nucleotide-gated channel A1 (CNGA1) (*B*); anti-Tα (GNAT1) (*C*); anti-cGMP phosphodiesterase (PDE6αβ) (*D*); anti-rhodopsin kinase (GRK1) (*E*); anti-prominin 1 (Prom1) (*F*); and anti-peripherin-2 (PRPH2) (*G*). *CC*, connecting cilium, equivalent to PTZ. *H–K*, normal trafficking of synaptic proteins. Sections were probed with: anti-Bassoon (*H*); anti-PSD95 (postsynaptic density protein 95) (*I*); anti-Ribeye (*J*); and anti-SV2 (synaptic vesicle protein) (*K*). *L* and *M*, synaptic terminal ultrastructure of P10 $^{emb}Kif3a^{+/-}$ (*L*) and $^{emb}Kif3a^{-/-}$ (*M*) cone pedicles. *N* and *O*, synaptic terminal ultrastructure of P10 $^{emb}Kif3a^{+/-}$ (*N*) and $^{emb}Kif3a^{-/-}$ (*O*) rod spherules.

$^{emb}Kif3a^{-/-}$ mice. The $^{emb}Kif3a^{-/-}$ retina developed ONL structure comparable with littermate controls through postnatal day 10 (P10) (Fig. 1, *B* and *C*). During elaboration of OS membrane and disc assembly at P10–11, the $^{emb}Kif3a^{-/-}$ ONL began to degenerate, first observed at P12. Degeneration continued through P14 and P21 and was complete at P24 (Fig. 1, *B* and *C*).

KIF3A localized to the IS and ONL of P6 and P10 $^{emb}Kif3a^{+/-}$ photoreceptors, but was undetectable by immunofluorescence in $^{emb}Kif3a^{-/-}$ photoreceptors (Fig. 1, *D* and *E*, *right*). P6 $^{emb}Kif3a^{-/-}$ retina lysate immunoblots detected low levels (<5%) of KIF3A (Fig. 1*F*, *left*), likely stemming from incomplete deletion of KIF3A in P6 peripheral $^{emb}Kif3a^{-/-}$ photoreceptors (47). At P6 (during PTZ formation), rhodopsin localized to the $^{emb}Kif3a^{+/-}$ perinuclear region (rough endoplasmic reticulum) and apical IS (Fig. 1*G*, *left*, *arrow*). In P6 predegenerate $^{emb}Kif3a^{-/-}$ retina, rhodopsin did not accumulate at the apical IS, but was distributed throughout the entire rod (Fig. 1*G*, *right*), indicating that trafficking was impeded. At P10, newly synthesized rhodopsin actively trafficked toward the $^{emb}Kif3a^{+/-}$ nascent ROS (Fig. 1*H*, *left*), whereas rhodopsin continued to accumulate in the $^{emb}Kif3a^{-/-}$ ONL and IS (Fig. 1*H*, *right*) as OS did not form. Rhodopsin protein levels of $^{emb}Kif3a^{+/-}$ (control) and $^{emb}Kif3a^{-/-}$ (mutant) retinas were comparable (Fig. 1*F*, *right*).

Immunolabeling with cone pigment-specific antibodies (S- and ML-opsins) revealed signal perinuclearly, as well over distal portions of nascent PTZs and pedicles of P6 $^{emb}Kif3a^{+/-}$ cones (Fig. 1, *I--L*, *left*). By P14, cone pigments localized exclusively to the COS of $^{emb}Kif3a^{+/-}$ retina (Fig. 1, *J–L*, *left*), whereas S- and ML-opsins were confined to somata and synaptic pedicles of P6 and P14 $^{emb}Kif3a^{-/-}$ cones (Fig. 1, *J–L*, *right*). All OS proteins examined, rod Tα (GNAT1), rod PDE6 (PDE6A, PDE6B), and rod CNG channel α-subunit (CNGA1), peripherin-2 (PRPH2), GC1 (GUCY2E), GCAP1 (GUCA1A), rhodopsin kinase (GRK1), and prominin 1 (Prom1), were absent from P10 $^{emb}Kif3a^{-/-}$ photoreceptor cortices (Fig. 2, *A–G*, *right*) but normally targeted to nascent OS in controls (Fig. 2, *A–G*, *left*). Synapse-associated proteins including Bassoon (BSN), PSD95 (DLG4), Ribeye (CTBP2), and synaptic vesicle glycoprotein 2 (SV2), were found correctly localized in the $^{emb}Kif3a^{-/-}$ photoreceptors (Fig. 2, *H–K*), suggesting that KIF3 is dispensable

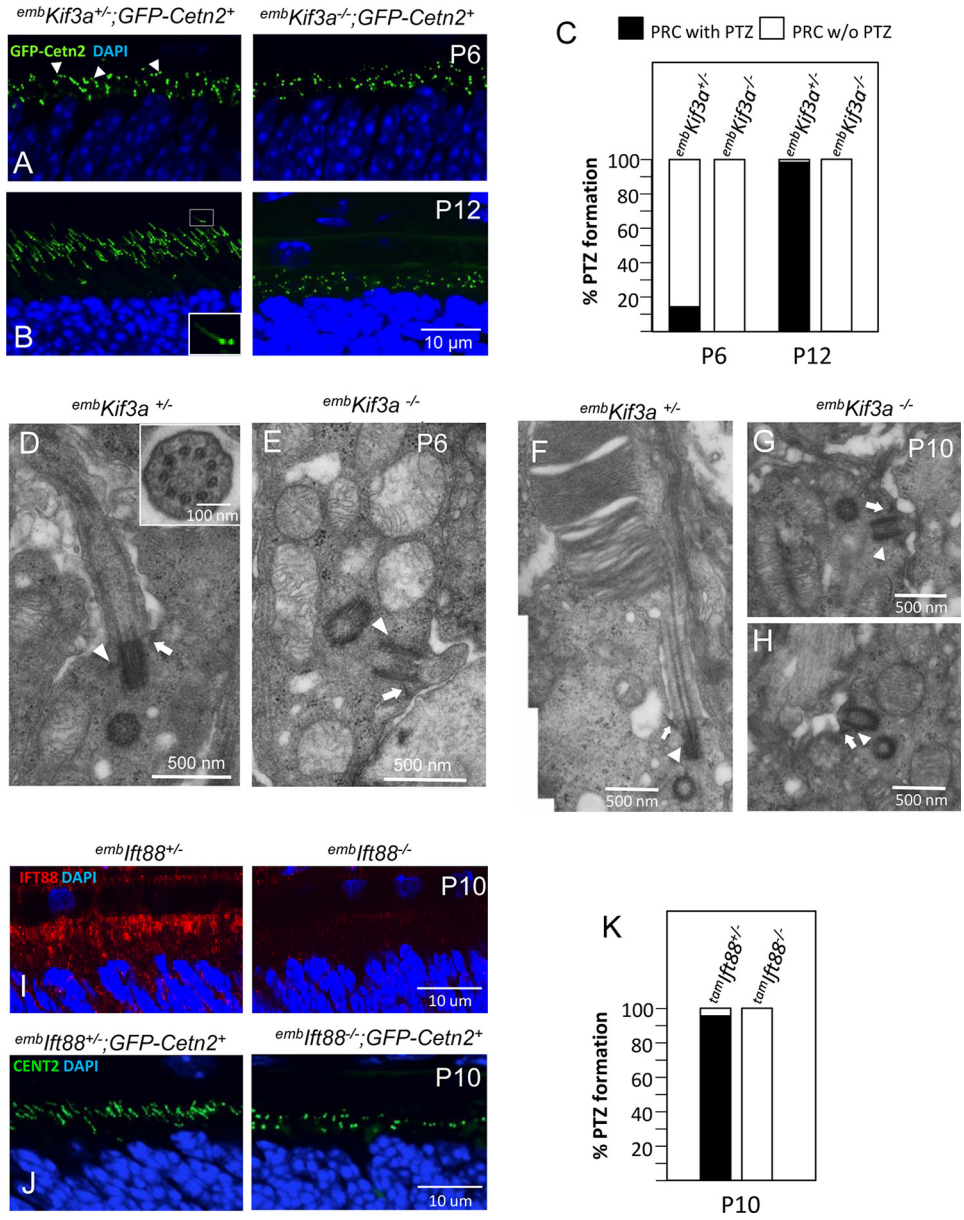

FIGURE 3. **Absence of PTZ formation in $^{emb}Kif3a^{-/-}$ and $^{emb}IFT88^{-/-}$ photoreceptors.** *A* and *B*, PTZ formation in $^{emb}Kif3a^{+/-}$;*Cetn2*$^{+}$ (*left*) and $^{emb}Kif3a^{-/-}$;*Cetn2*$^{+}$ (*right*) photoreceptors visualized with centriole/PTZ marker GFP-CENT2 at P6 (*A*) and P12 (*B*). In $^{emb}Kif3a^{+/-}$ photoreceptors, centrioles appear as green dots, and PTZs appear as 1 μm-long green streaks resembling shooting stars. Note that centrioles, but not PTZs, were observed in $^{emb}Kif3a^{-/-}$ photoreceptors. *C*, the percentage of PTZ formation in $^{emb}Kif3a^{+/-}$;*Cetn2*$^{+}$ and $^{emb}Kif3a^{-/-}$;*Cetn2*$^{+}$ photoreceptors (*PRC*) (100–150 photoreceptors each) at P6 and P12. *D–H*, $^{emb}Kif3a^{+/-}$ and $^{emb}Kif3a^{-/-}$ photoreceptor ultrastructure. *D*, P6 $^{emb}Kif3a^{+/-}$ photoreceptor with basal body, daughter centriole, and PTZ. The *inset* shows a cross-section of the basal body with nine microtubule doublets. *E*, $^{emb}Kif3a^{-/-}$ photoreceptor with basal body docked to the cell membrane, lacking a PTZ. *F*, P10 $^{emb}Kif3a^{+/-}$ photoreceptor with stacks of membrane discs forming at the connecting cilium distal portion. However, in $^{emb}Kif3a^{-/-}$ photoreceptors, mother centrioles dock to the cortex normally but are devoid of PTZ and OS at P6 (*E*) and P10 (*G* and *H*). Mother centriole subdistal (*arrow*) and distal (*arrowhead*) appendages are indicated. *I*, P10 $^{emb}Ift88^{+/-}$ (*left*) and $^{emb}Ift88^{-/-}$ (*right*) retina cryosections probed with anti-IFT88 antibody (*red*). *J*, P10 $^{emb}Ift88^{+/-}$;*Cetn2*$^{+}$ (*left*) and $^{emb}IFT88^{-/-}$;*Cetn2*$^{+}$ (*right*) sections. PTZ formation is detected by transgenic GFP-CENT2 forming streaks in $^{emb}Ift88^{+/-}$;*Cetn2*$^{+}$, but not $^{emb}Ift88^{-/-}$;*Cetn2*$^{+}$ photoreceptors. *K*, the percentage of PTZ formation in $^{emb}Ift88^{+/-}$;*Cetn2*$^{+}$ and $^{emb}Ift88^{-/-}$;*Cetn2*$^{+}$ photoreceptors (100–150 photoreceptors each) at P10.

for synaptic terminal development and protein transport. Ultrastructural examination of $^{emb}Kif3a^{-/-}$ and $^{emb}Kif3a^{+/-}$ photoreceptors revealed that rod spherules and cone pedicles form normally, and ribbon structures were similar between genotypes (Fig. 2, *L–O*).

Abrogated Ciliogenesis in $^{emb}Kif3a^{-/-}$ Photoreceptors—We investigated PTZ formation by fluorescence labeling with transgenic GFP-tagged CETN2. CETN2 (centrin 2) is a Ca^{2+}-binding protein associated with photoreceptor centrioles and PTZs (48, 49). Transgenic GFP-CETN2 fusion protein (43) expressed in $^{emb}Kif3a^{-/-}$;*GFP-Cetn2*$^{+}$ mice monitors the presence of centrioles and PTZs (Fig. 3, *A* and *B*). In P6 control mice, photoreceptor centrioles were visible as paired green dots at apical IS regions adjacent to the RPE. Among the small dots, several nascent PTZs are shown as short green lines (Fig. 3*A*, *left*, *arrowheads*), amounting to fewer than 20% of all basal bodies (Fig. 3*C*). By P12, fully developed PTZs are present (~1 μm in length), each paired with a daughter centriole at its base

("shooting star," Fig. 3*B*, *left panel*, *inset*). Apart from numerous centriolar pairs, no GFP-CENT2-labeled PTZs are detectable in $^{emb}Kif3a^{-/-}$ photoreceptor apical ISs (Fig. 3, *A* and *B*, *right*, and 3*C*).

The absence of GFP-CETN2-labeled PTZs in P12 $^{emb}Kif3a^{-/-}$ rods prompted us to examine the ultrastructure of $^{emb}Kif3a^{-/-}$ PTZs and centrioles. In P6 $^{emb}Kif3a^{+/-}$ controls, we observed PTZ "buds" protruding from one basal body anchored at the photoreceptor cortex with subdistal and distal appendages (Fig. 3*D*, *arrow* and *arrowhead*, respectively). By P10, nascent OSs containing stacks of membrane discs appear at the PTZ distal portion (Fig. 3*F*). However, in $^{emb}Kif3a^{-/-}$ photoreceptors, basal bodies docked at the apical IS with normal centriolar appendages (Fig. 3*E*, *arrow* and *arrowhead*), but failed to extend axonemes toward PTZ development at P6 (Fig. 3*E*) and toward OS at P10 (Fig. 3, *G* and *H*). Both photoreceptor ultrastructure and GFP-CETN2 labeling indicate aborted ciliogenesis in $^{emb}Kif3a^{-/-}$ photoreceptors, thereby linking KIF3 to transition zone formation. The transition zone has been proposed as a gate for ciliary protein trafficking in primary cilia (50).

IFT Drives PTZ and Outer Segment Formation—A recent study of mouse embryonic fibroblasts revealed that KIF3 during initial stages of ciliogenesis assumes a novel role in centriolar organization that is distinct from its IFT motor function (51). In the absence of KIF3A, subdistal appendages, microtubule anchoring, and basal foot formation were abrogated. It is therefore important to discriminate the role of KIF3 in transition zone formation via IFT or its non-IFT organization of centriolar subdistal appendages organization. We disrupted photoreceptor IFT by deletion of IFT88, a critical subunit of the IFT-B complex that is essential for proper IFT in *C. elegans* (52, 53), *Chlamydomonas* (14), *Xenopus* (54), mouse (17), and humans (55). By crossing an *Ift88* floxed mouse line (36) with Six3Cre mice, we generated $Ift88^{f/f};Six3Cre^{+}$ ($^{emb}Ift88^{-/-}$) mice in which anterograde IFT is disabled in photoreceptor progenitors. We verified the absence of IFT88 in P10 $^{emb}Ift88^{-/-}$ photoreceptors by immunohistochemistry using an anti-IFT88 antibody (Fig. 3*I*), and assayed for PTZ formation in $^{emb}Ift88^{-/-};GFP\text{-}Cetn2^{+}$ photoreceptors (Fig. 3*J*). Similar to the *Kif3a* mutant (Fig. 3*B*), PTZs failed to form at the apical ISs of P10 $^{emb}Ift88^{-/-}$ photoreceptors (Fig. 3*J*, *right*, and 3*K*) confirming that photoreceptor PTZ formation and subsequent OS development require KIF3-driven IFT.

KIF3A Depletion in the Adult Mouse Causes Outer Segment Degeneration—A rod-specific *Kif3a* knock-out showed that rhodopsin trafficked to the OS even as the OS degenerated (32). However, KIF3 and IFT88 were associated with rhodopsin trafficking in cultured hTert-RPE1 cells (56), and rhodopsin was pulled down by IFT88 together with GC1 as IFT cargo (21), suggesting the involvement of KIF3 in rhodopsin trafficking. To solve this apparent discrepancy, we deleted KIF3A in the adult mouse using a tamoxifen-inducible *Cre/loxP* recombination system, *CAG-CreER* (38) (Fig. 4*A*). We induced nuclear translocation of *CreER* with tamoxifen on 5 consecutive days and followed the rate of degeneration in cryosections for 8 weeks (Fig. 4, *C* and *D*). $Kif3a^{f/-};CreER^{+}$ ($^{tam}Kif3a^{-/-}$) photoreceptors degenerated progressively, but the rate of degeneration was slower and less severe than that occurring in $^{emb}Kif3a^{-/-}$ mice (Fig. 1, *B* and *C*). No morphological defects were obvious in the $^{tam}Kif3a^{-/-}$ mouse retinas at 2 and 3 weeks post-tamoxifen induction (PTI), whereas the OS shortened at 4 weeks PTI and degeneration progressed with >90% reduced photoreceptor OS and ONL thicknesses by 7 and 8 weeks PTI (Fig. 4, *C* and *D*).

Rhodopsin and OS Proteins Traffic to $^{tam}Kif3a^{-/-}$ Photoreceptor Outer Segments in the Absence of KIF3—If rhodopsin trafficking to outer segments requires KIF3, depletion of KIF3A should prevent rhodopsin trafficking to the ROS. After five consecutive daily inductions of $Kif3a^{f/-};CreER^{+}$ mice with tamoxifen, KIF3A was undetectable by immunohistochemistry in the $^{tam}Kif3a^{-/-}$ photoreceptors as early as 1 week PTI (Fig. 4*E*, *right*) and undetectable by immunoblot at 2 weeks PTI (Fig. 4*B*). KIF3A levels were unchanged in $^{tam}Kif3a^{-/+}$ controls (Fig. 4, *E*–G, *left*). Rhodopsin localized normally in $^{tam}Kif3a^{-/-}$ ROS at 1 and 2 weeks PTI (Fig. 4, *H* and *I*, *right*), a time interval during which ROS disc membranes should have been replaced completely (57). By 3 weeks PTI, when the $^{tam}Kif3a^{-/-}$ OS layer was shortened more than 50% (Fig. 4*J*, *right*) relative to controls (Fig. 4*J*, *left*), rhodopsin was still localized correctly to the ROS, although minor mislocalization of rhodopsin became obvious (Fig. 4*J*, *arrows*). ML- and S-opsins were targeted correctly to the $^{tam}Kif3a^{-/-}$ COSs up to 3 weeks PTI (Fig. 4, *K*–*P*, *right*), similar to the $^{tam}Kif3a^{-/+}$ controls. However, cone opsins started to be retained in inner segments and mistrafficked to synaptic termini at 2 weeks PTI (Fig. 4, *L* and *O*, *right*, *arrows*), earlier than seen for rhodopsin. Cone pigment mislocalization only became severe after 3 weeks PTI (Fig. 4, M and P, *right*).

Scotopic $^{tam}Kif3a^{-/-}$ photoreceptor function appeared normal at 1 and 2 weeks PTI, but electroretinogram a- and b-wave amplitudes were reduced as $^{tam}Kif3a^{-/-}$ OSs shortened at 3 weeks PTI (Fig. 5, *A*–*C*, note 3-week trace, *red*, in Fig. 5*B*). Photopic responses of $^{tam}Kif3a^{-/-}$ retinas were present at 1, 2, and 3 weeks PTI, and were first attenuated at 2 weeks PTI (Fig. 5, *A* and *B*).

Other membrane and membrane-associated proteins, including GC1, CNGA1, PDE6, and peripherin-2, trafficked normally in $^{tam}Kif3a^{-/-}$ photoreceptors within the first 2 weeks PTI (Fig. 6, *A*, *C*, *E*, and *G*, *right*). At 3 weeks PTI, photoreceptor OSs shortened and started to disintegrate, causing mislocalization of these polypeptides (Fig. 6, *B*, *D*, *F*, and *H*, *right*). Peripherin-2 (Fig. 6*F*) and PDE6 (Fig. 6*H*) were more severely affected in the $^{tam}Kif3a^{-/-}$ photoreceptors than GC1 (Fig. 6*B*) and CNGA1 (Fig. 6*D*) polypeptides. These results suggest that KIF3 is nonessential for trafficking of membrane-associated proteins to rod and cone OSs.

S-opsin Trafficking to $Rho^{-/-};{}^{tam}Kif3a^{-/-}$ Rod Outer Segments—To test whether the early-onset cone opsin mislocalization at IS and synaptic termini is due to morphological differences between rod and cone photoreceptor OSs, we expressed S-opsin in mouse rod photoreceptors under the control of the rhodopsin promoter in $Rho^{-/-};{}^{tam}Kif3a^{-/-}$ and $Rho^{+/-};{}^{tam}Kif3a^{-/-}$ backgrounds. Native ML-opsin still mislocalized in the cone ISs and synaptic termini of both $S\text{-}opsin^{+};Rho^{+/-};{}^{tam}Kif3a^{-/-}$ (Fig. 7*A*, *right*) and $S\text{-}opsin^{+};Rho^{-/-};{}^{tam}Kif3a^{-/-}$ (Fig. 7, *C* and *E*, *right*) mouse retinas at 2 and 3

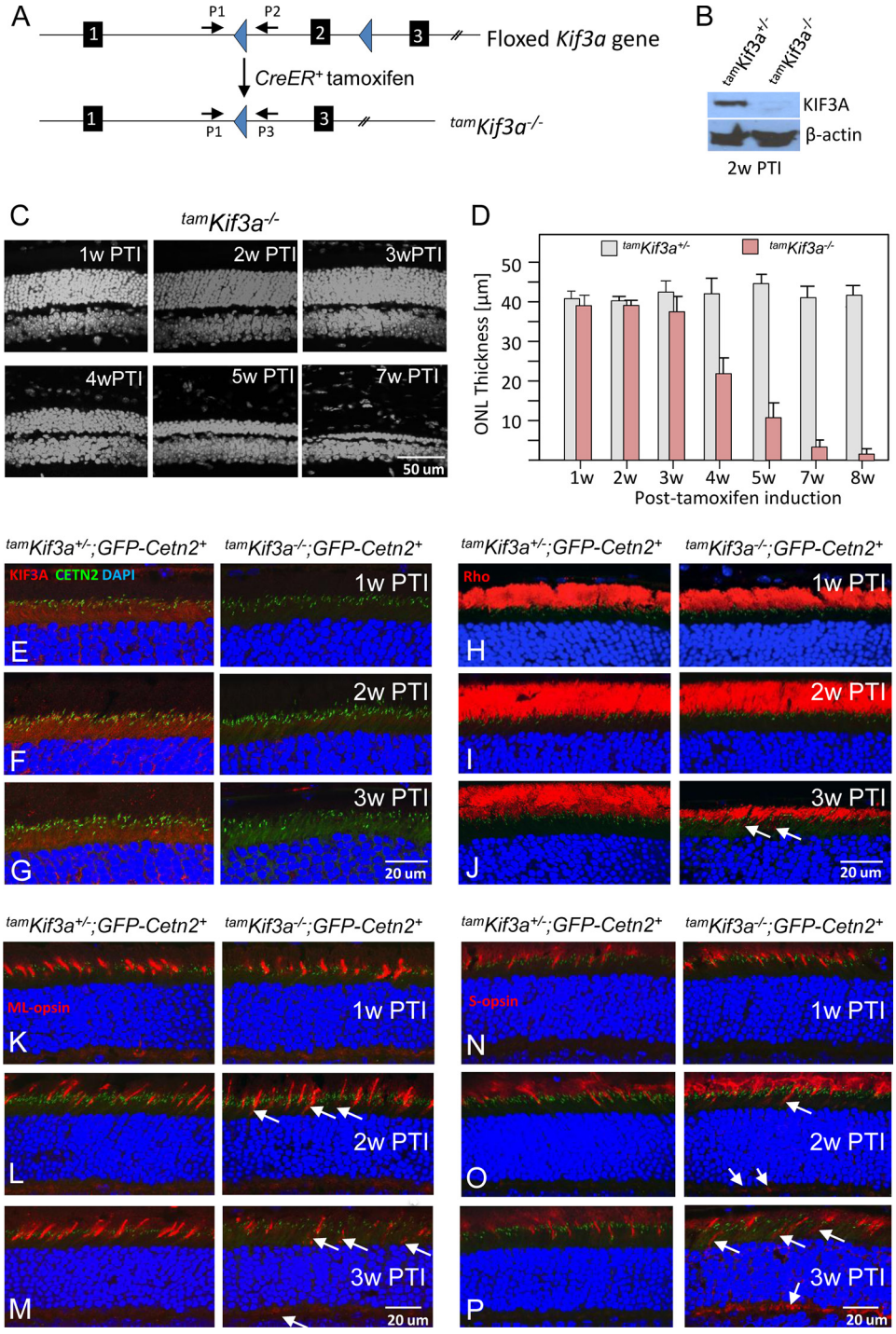

FIGURE 4. **Photoreceptor degeneration in $^{tam}Kif3a^{-/-}$ retina.** *A*, *Kif3a* knockouts ($^{tam}Kif3a^{-/-}$) generated by intraperitoneal tamoxifen induction of $Kif3a^{flox/flox}$;$CreER^{+}$ mice. *B*, Western blot of $^{tam}Kif3a^{+/-}$ (*left*) and $^{tam}Kif3a^{-/-}$ (*right*) retina lysate at 2 weeks PTI (*2w PTI*) probed with anti-KIF3A antibody. β-Actin was used as a loading control. *C*, representative retina transverse sections at 1 week post-tamoxifen injection (*1w PTI*) to 7 weeks PTI (*7w PTI*). *D*, quantitation of ONL thickness (in μm) of heterozygous and homozygous knockouts from 1–8 weeks post-tamoxifen injection. *Error bars* indicate mean ± S.E. *E–G*, in $^{tam}Kif3a^{+/-}$ (*left*) and $^{tam}Kif3a^{-/-}$ (*right*) sections probed with anti-KIF3A antibody (*red*) at 1 week (*E*), 2 weeks (*F*), and 3 weeks (*G*) PTI; KIF3A (*red*) appears absent in $^{tam}Kif3a^{-/-}$ photoreceptors as early as 1 week PTI. *H–J*, $^{tam}Kif3a^{+/-}$ (*left*) and $^{tam}Kif3a^{-/-}$ (*right*) sections probed with anti-rhodopsin (*red*) antibody. Rhodopsin (*red*) traffics normally at 1 week (*H*) and 2 weeks (*I*) PTI, but at 3 weeks, $^{tam}Kif3a^{-/-}$ ROS appear shortened and rhodopsin appear mislocalized (*J*, *right*, *white arrows*). *K–P*, immunolocalization of ML- and S-opsins in $^{tam}Kif3a^{+/-}$;$Cetn2^{+}$ (*left*) and $^{tam}Kif3a^{-/-}$;$Cetn2^{+}$ (*right*) cones at 1 week (*K* and *N*), 2 weeks (*L* and *O*), and 3 weeks (*M* and *P*) PTI. At 2 weeks PTI, cone opsins mislocalize in $^{tam}Kif3a^{-/-}$ cone inner segments and synaptic termini (*right*, *arrows*).

weeks PTI as seen in $^{tam}Kif3a^{-/-}$ mice (Fig. 4*P*, *right*). However, ectopically expressed S-opsin traffics to the *S-opsin*$^{+}$;*Rho*$^{+/-}$;$^{tam}Kif3a^{-/-}$ rod OSs Fig. 7*B*, *right*) and the *S-opsin*$^{+}$;*Rho*$^{-/-}$;$^{tam}Kif3a^{-/-}$ rod OS (Fig. 7*D*, *right*) at 2 weeks PTI. Retinal degeneration was more severe in *Rho*$^{-/-}$ mice due to loss of rhodopsin. By 3 weeks PTI, transgenic S-opsin still trafficked to the rod OS, and mistrafficking observed (Fig. 7*F*, *right*, *arrows*) may be caused by endogenous S-opsin in *S-opsin*$^{+}$;*Rho*$^{-/-}$;$^{tam}Kif3a^{-/-}$ cones. This suggests that different rod/cone axoneme sub-structures may account for earlier cone opsin mistrafficking in cones.

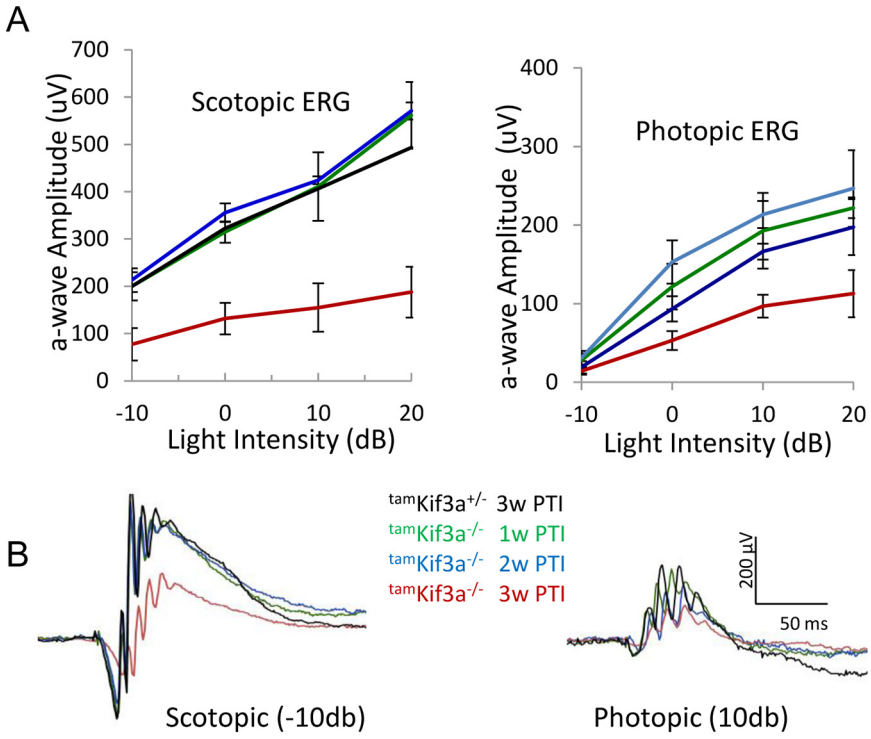

C

Light intensity (dB)	-10	0	10	20	*P-value*
	a-wave amplitude of scotopic ERG response (uV)				
Het_1w PTI	193±28	319±52	430±37	530±56	0.85
KO_1w PTI	200±30	315±23	411±72	561±71	
Het_2w PTI	226±40	314±70	445±33	630±50	0.03
KO_2w PTI	213±25	356±20	424±8	571±18	
Het_3w PTI	200±22	323±19	406±59	493±88	<0.001*
KO_3w PTI	77±35	132±33	155±51	188±54	
	b-wave amplitude of photopic ERG response (uV)				
Het_1w PTI	27±8	138±16	213±25	238±50	0.29
KO_1w PTI	28±9	122±29	193±48	222±13	
Het_2w PTI	25±4	159±48	213±67	273±71	0.005*
KO_2w PTI	19±8	93±16	166±10	197±36	
Het_3w PTI	31±9	153±27	213±17	246±49	<0.001*
KO_3w PTI	14±4	53±12	97±15	113±30	

*P-value<0.01

FIGURE 5. **Scotopic and photopic ERG responses of ^{tam}*Kif3a*$^{+/-}$ and ^{tam}*Kif3a*$^{-/-}$ mice.** *A*, scotopic a-wave amplitudes (*left panel*) and photopic b-wave amplitudes (*right panel*) as a function of light intensity (*right panel*). ^{tam}*Kif3a*$^{+/-}$ served as a control. *Error bars* indicate mean ± S.E. *B*, scotopic (−10 db) and photopic (10 db) ERG responses from control ^{tam}*Kif3a*$^{+/-}$ controls and ^{tam}*Kif3a*$^{-/-}$ mice at 1 week PTI (*1w PTI*, *green traces*), 2 weeks PTI (*2w PTI*, *blue traces*), and 3 weeks PTI (*3w PTI*, *red traces*) PTI. *C*, statistical analysis of a- and b-wave amplitudes at 1–3 weeks PTI. *Het*, heterotrimeric.

Rhodopsin Trafficking Is Independent of IFT88—Excluding a possibility that IFT transports rhodopsin via motor(s) other than kinesin-2 proteins, we disabled anterograde IFT by depletion of IFT88, a core component of IFT-B protein complexes that moves cargo from the ciliary base to the axoneme tip. We generated a ^{tam}*Ift88*$^{-/-}$ (*Ift88*$^{f/-}$;*CreER*$^{+}$) mouse line, conditionally disrupting IFT88 function in mature photoreceptors by tamoxifen-induced gene targeting. IFT88 localizes to the inner segment myoid region of heterozygous ^{tam}*Ift88*$^{+/-}$ photoreceptors (Fig. 8*A*). In ^{tam}*Ift88*$^{-/-}$ photoreceptors, IFT88 was undetectable 3–5 weeks PTI (Fig. 8*B*). Rhodopsin trafficking, however, appeared unaffected by the absence of IFT88. Rhodopsin was present in ^{tam}*Ift88*$^{-/-}$ OSs at 3 and 4 weeks PTI and only mislocalized in inner segments at 5 weeks PTI, a time when ROS structure has disintegrated and lost 90% of length (Fig. 8*C*) relative to the heterozygous control. This result suggests that rhodopsin transport occurs independently of IFT driven by plus-oriented molecular motors.

Axoneme Maintenance in Mature Photoreceptors Requires Kif3A—Fluorescence microscopy of the GFP-CENT2-labeled ^{tam}*Kif3a*$^{-/-}$ connecting cilia (Fig. 9, *A*–*C*, *right*) revealed normal basal body-connecting cilia shooting star arrangements, as observed in controls (Fig. 9, *A*–*C*, *left*). Even at 3 weeks PTI, when OSs in the inducible knockouts were shortened more than 50%, PTZs appeared normal (Fig. 9*D*).

Based on OS shortening at 3 weeks PTI (Fig. 4*J* and Fig. 6, *B*, *D*, *F*, and *H*, *right*), we suspected that KIF3a depletion in mature photoreceptors would first affect the axoneme structure at the OS distal tip. To test this hypothesis, we examined OS axonemes by immunostaining with antibodies directed against axoneme-specific microtubule proteins, RP1 and Ac-α-tubulin. RP1 is a microtubule-associated protein (MAP) that stabilizes

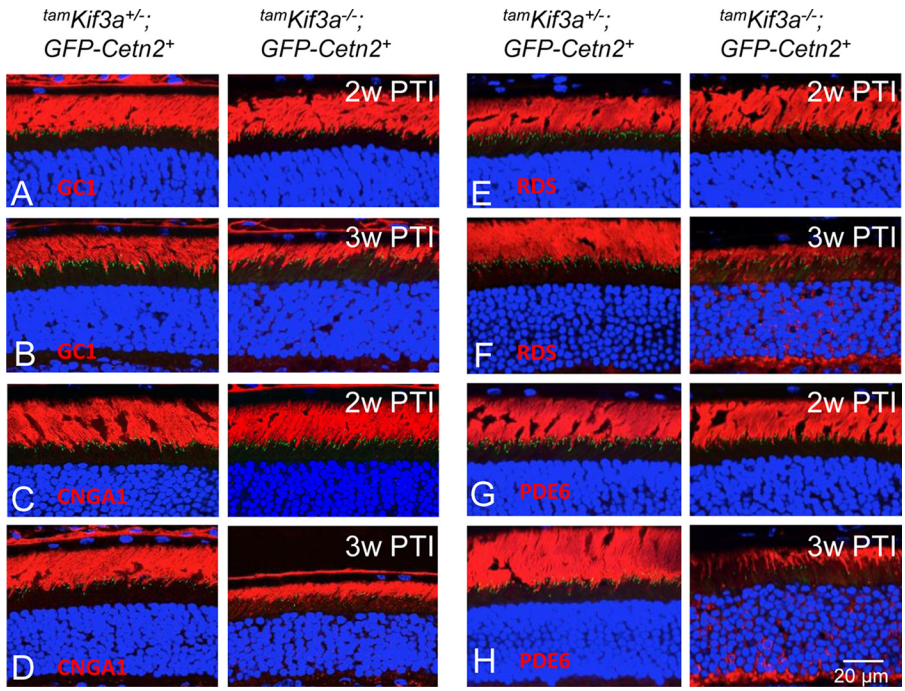

FIGURE 6. **Protein trafficking in $^{tam}Kif3a^{-/-}$ photoreceptors.** *A–H*, immunolocalizations of membrane and membrane-associated proteins in $^{tam}Kif3a^{+/-}$ (*left*) and $^{tam}Kif3a^{-/-}$ (*right*) photoreceptors at 2 and 3 weeks PTI. *A* and *B*, GC1; *C* and *D*, CNGA1; *E* and *F*, RDS (peripherin-2); and *G* and *H*, PDE6. These proteins mislocalize in the $^{tam}Kif3a^{-/-}$ IS, ONL and OPL at 3 weeks PTI, coincident with OS shortening.

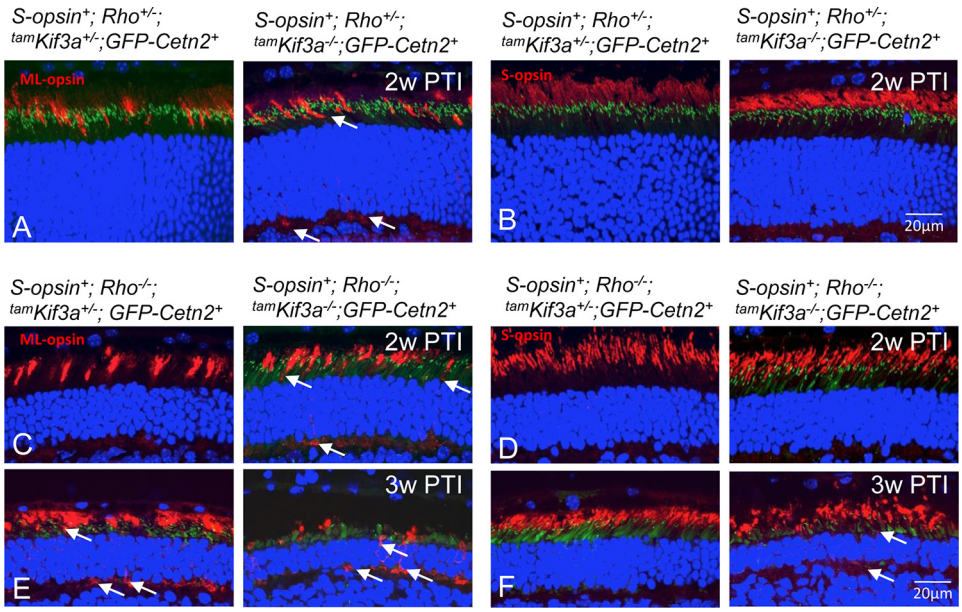

FIGURE 7. **Trafficking of ectopically expressed S-opsin in rods.** *A* and *B*, $^{tam}Kif3a^{+/-}$ and $^{tam}Kif3a^{-/-}$ sections ($Rho^{+/-}$ background) probed with anti-ML-opsin (*A*) and S-opsin (*B*) antibodies. The mice also express S-opsin under control of the rhodopsin promoter and GFP-CETN2 under the CAG promoter. At 2 weeks PTI (*2w PTI*), native ML-opsin mislocalizes in ISs and synaptic termini of *S-opsin*$^{+}$;$Rho^{+/-}$;$^{tam}Kif3^{-/-}$;*GFP-Cetn2*$^{+}$ cone photoreceptors (*A*, *right*, *arrows*), but targets to COS in *S-opsin*$^{+}$;$Rho^{+/-}$;$^{tam}Kif3^{+/-}$;*GFP-Cetn2*$^{+}$ (*A*, *left*). In contrast, transgenic S-opsin traffics normally to ROS in *S-opsin*$^{+}$;$Rho^{+/-}$;$^{tam}Kif3^{-/-}$;*GFP-Cetn2*$^{+}$ and *S-opsin*$^{+}$;$Rho^{+/-}$;$^{tam}Kif3a^{+/-}$;*GFP-Cetn2*$^{+}$ mice. *C–F*, 2 weeks PTI (*2w PTI*) $^{tam}Kif3a^{+/-}$ and $^{tam}Kif3a^{-/-}$ (*C* and *D*) and 3 weeks PTI (*3w PTI*) $^{tam}Kif3a^{+/-}$ and $^{tam}Kif3a^{-/-}$ (*E* and *F*) sections on a $Rho^{-/-}$ and *GFP-Cetn2*$^{+}$ background probed with antibodies directed against ML-opsin (*C* and *E*) and S-opsin (*D* and *F*). In *S-opsin*$^{+}$;$Rho^{-/-}$;$^{tam}Kif3^{-/-}$;*GFP-Cetn2*$^{+}$ mice at 2 weeks PTI, ML-opsin mislocalizes at cone IS and synaptic terminal regions (*C*, *right*), whereas transgenic S-opsin traffics normally to ROS (*D*, *right*). By 3 weeks PTI, both ML-opsins (*E*, *right*) and S-opsins (*F*, *right*) mislocalize in IS and synaptic terminal regions of *S-opsin*$^{+}$;$Rho^{-/-}$;$^{tam}Kif3^{-/-}$;GFP-Cetn2^{+} photoreceptors as structure is disrupted severely. ML-opsin mislocalization was also observed in the heterozygous control at 3 weeks (*E*, *left*), but not at 2 weeks (*C*, *left*) PTI. No mistrafficking of transgenic S-opsin was observed in heterozygous control rods at 2 weeks PTI (*D*, *left*), but mistrafficking occurred in depleted retinas at 3 weeks PTI (*F*, *right*, *arrows*).

the axoneme (58, 59). At 1 week PTI, OS axonemes labeled with anti-RP1 antibody were found shorter in most of the $^{tam}Kif3a^{-/-}$ photoreceptors (Fig. 9*E*, *right*) when compared with those in the $^{tam}Kif3a^{-/+}$ control (Fig. 9*E*, *left*). At 2 weeks PTI, $^{tam}Kif3a^{-/-}$ axoneme shortening was more severe (Fig. 9*F*, *right*), and by 3 weeks PTI OSs and axonemes were severely shortened and disrupted (Fig. 9*G*, *right*). Quantitative analysis shows that the lengths of the $^{tam}Kif3a^{-/-}$ axoneme are less than

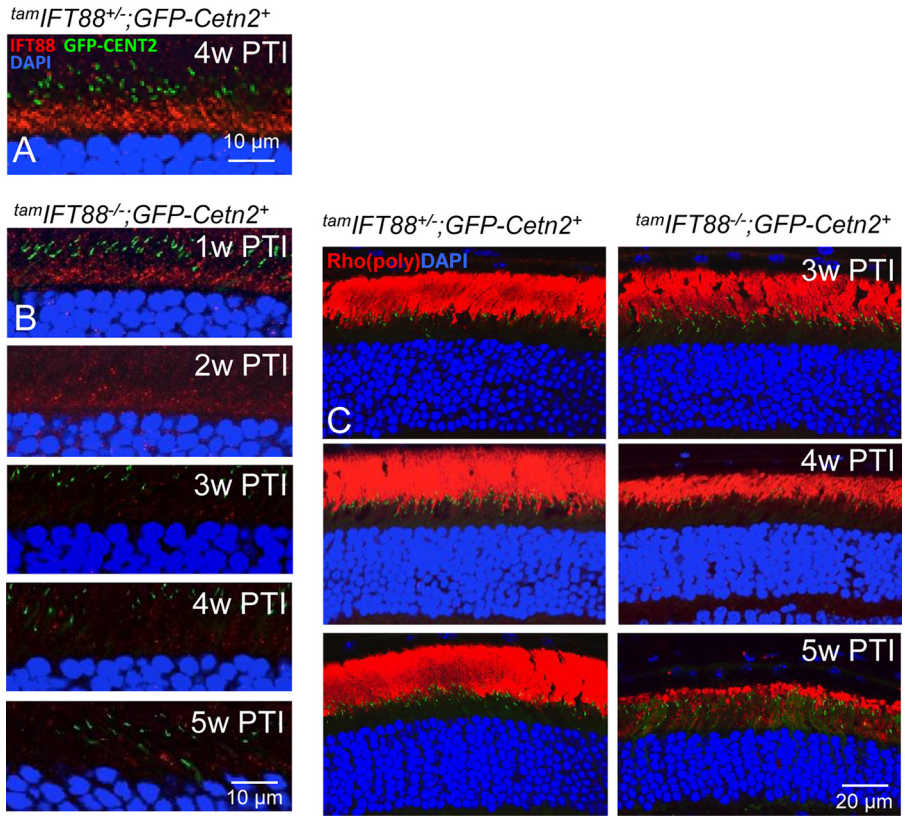

FIGURE 8. **Rhodopsin traffics after tamoxifen-induced depletion of IFT88 in adult photoreceptors.** *A* and *B*, ^{tam}*Ift88a*$^{+/-}$;*GFP-Cetn2*$^{+}$ (*A*) and ^{tam}*Ift88a*$^{-/-}$;*GFP-Cetn2*$^{+}$ (*B*) cryosections probed with anti-IFT88 antibody. IFT88 is expressed in ^{tam}*Ift88a*$^{+/-}$ photoreceptor ISs at 4 weeks PTI (*4w PTI*) (*A*), as well as weakly in ^{tam}*Ift88a*$^{-/-}$ (*B*) at 1 week (*1w*) and 2 weeks (*2w*) PTI. No IFT88 is detected in 3–5 weeks PTI ^{tam}*Ift88a*$^{-/-}$ photoreceptors. In *panel B*, please note that the 2 weeks PTI section is *GFP-Cetn2*$^{-}$ (no *Cetn2* transgene). *C*, rhodopsin (*Rho*) (*red*) localization in ^{tam}*Ift88a*$^{+/-}$ (*left*) and ^{tam}*Ift883a*$^{-/-}$ (*right*) rods at 3, 4, and 5 weeks PTI. Rhodopsin mislocalizes in ^{tam}*Ift88a*$^{-/-}$ rod inner segment (RIS) at 5 weeks PTI when ROS degenerate.

⅓ of those of heterozygotes (Fig. 9*H*). A similar result was obtained with anti-Ac-α-tubulin antibody staining. PTZs and axonemes of control retinas were correctly elaborated (Fig. 9*I*, *left*), whereas at 1 week PTI, ^{tam}*Kif3a*$^{-/-}$ axonemes disintegrated and Ac-α-tubulin accumulated in the cone IS (Fig. 9*I*, *right*). At 2 weeks PTI, OSs and axonemes were completely disorganized (Fig. 9*J*, *right*).

By ultrastructure at 2 weeks PTI, ^{tam}*Kif3a*$^{-/-}$ mice show normal rod and cone elaboration of the PTZ and OSs (Fig. 10, *C* and *D*) as the ^{tam}*Kif3*$^{+/-}$ control (Fig. 10, *A* and *B*). However, ^{tam}*Kif3a*$^{-/-}$ cone photoreceptors exhibited cytoplasmic condensation indicative of imminent cell death (Fig. 10*D*). ^{tam}*Kif3a*$^{-/-}$ rods, in contrast, showed normal structure and no cytoplasm condensation consistent with electroretinogram and histology results. When compared with ^{emb}*Kif3a*$^{-/-}$ retina, ^{tam}*Kif3a*$^{-/-}$ cone-rod degeneration was less severe. These results suggest that KIF3A is essential for axoneme maintenance and photoreceptor survival.

DISCUSSION

Under conditions of normal development, the basal body docks to the inner segment cortex during late ciliogenesis, with subdistal appendages forming the basal foot for microtubule anchoring and IFT beginning to deliver ciliary proteins. Extension of ciliary stalks and OS formation usually initiate around P3 and P7, respectively (60). Our results show that deletion of KIF3A or IFT88 in retinal progenitors prevented photoreceptor PTZ, axoneme, and OS formation, thus aborting ciliogenesis after the basal body docked to cell membrane. Expression of basal body/PTZ marker GFP-CETN2 in ^{emb}*Kif3a*$^{-/-}$ mice (Fig. 3, *A* and *B*) and ultrastructure of ^{emb}*Kif3a*$^{-/-}$ photoreceptors (Fig. 3, *D–H*) demonstrated the absence of PTZs and axonemes, although basal bodies docked to the cell membrane correctly (Fig. 3, *E*, *G*, and *H*). These experiments demonstrate that KIF3-dependent IFT is necessary for axoneme and PTZ formation. The ^{emb}*Ift88*$^{-/-}$ phenotype is distinct from that of the Oak Ridge Polycystic Kidney (ORPK) mouse carrying a hypomorphic mutation in the Ift88 gene. ORPK mice form normal PTZs but elaborate short disorganized OS and retinal degeneration. In the ^{emb}*Ift88*$^{-/-}$ mouse, PTZs and axonemes never formed. In the ^{emb}*Ift88*$^{-/-}$ and ^{emb}*Kif3a*$^{-/-}$ photoreceptors, membrane proteins destined to traffic to outer segments backed up in the inner segment, similarly as seen in KIF3A deletion based on early *Cre* expression driven by the interstitial retinoid binding protein (IRBP) promoter (29). Photoreceptor degeneration started at P12, when OSs rapidly developed in WT photoreceptors, and the degeneration was complete 2 weeks later (Fig. 1, *B* and *C*). Consequently, IFT mediated by KIF3 and IFT88 is required for PTZ formation and axoneme extension.

In a second experimental series, we depleted KIF3A or IFT88 in fully developed photoreceptors by tamoxifen-induced gene targeting (Fig. 4). We focused on primary defects of either outer segment morphology or membrane protein trafficking. KIF3A

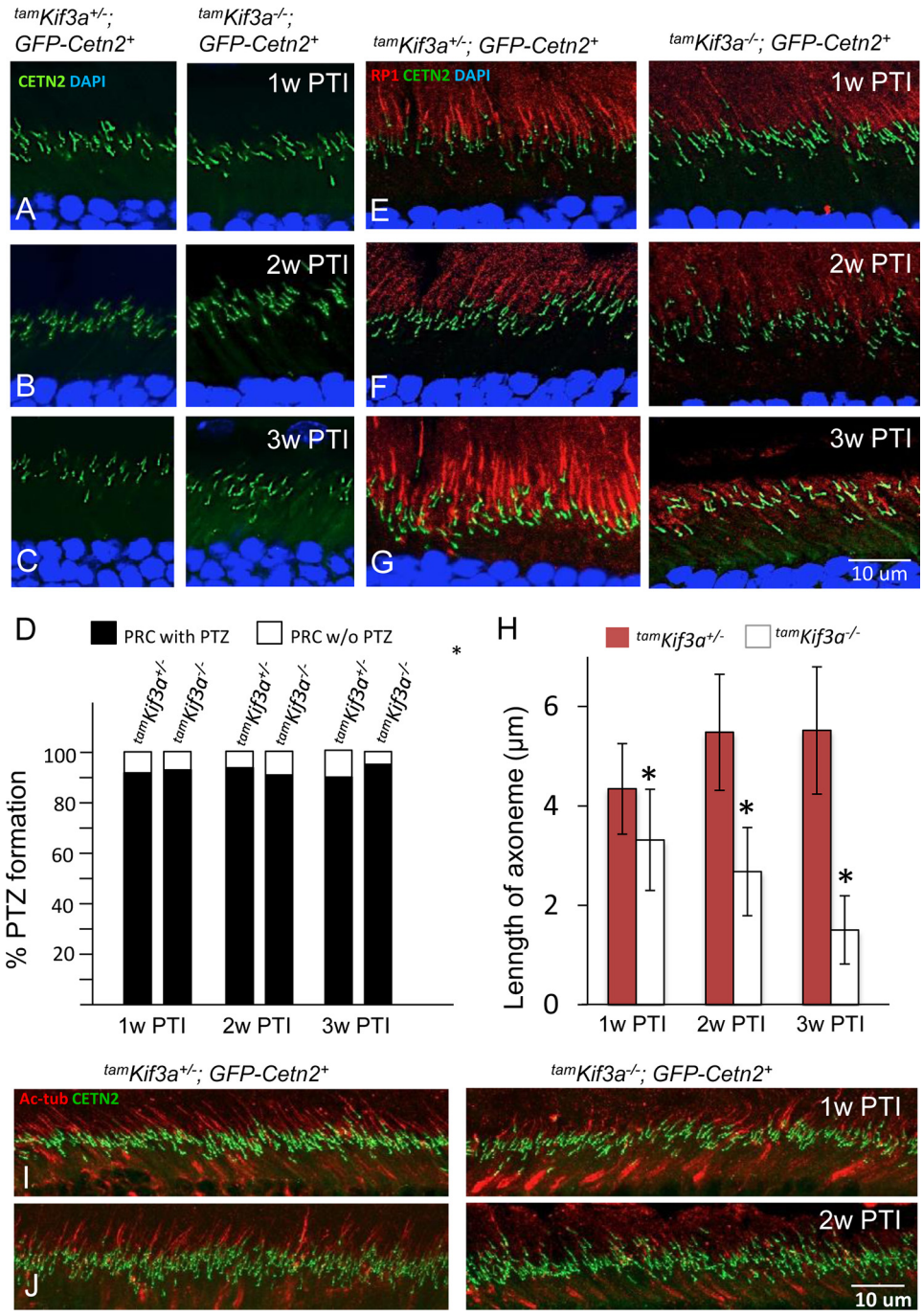

FIGURE 9. **Intact PTZ, but deteriorating distal axonemes in adult KIF3A-depleted photoreceptors.** *A–C*, $^{tam}Kif3a^{+/-}$;*Gfp-Cent2*$^{+}$ and $^{tam}Kif3a^{-/-}$;*Gfp-Cent2*$^{+}$ sections at 1 week (*1w*) (*A*), 2 weeks (*2w*) (*B*), and 3 weeks (*3w*) (*C*) PTI. Note that *Gfp-Cent2*-labeled PTZ (1-μm green lines) are intact in $^{tam}Kif3a^{-/-}$ photoreceptors (*right*). *D*, the percentage of PTZ formation in $^{tam}Kif3a^{+/-}$;*Cetn2*$^{+}$ and $^{tam}Kif3a^{-/-}$;*Cetn2*$^{+}$ photoreceptors (100 photoreceptors each) at 1, 2, and 3 weeks PTI. *E–G*, $^{tam}Kif3a^{+/-}$;*Gfp-Cent2*$^{+}$ and $^{tam}Kif3a^{-/-}$;*Gfp-Cent2*$^{+}$ axonemes labeled with anti-RP1 antibody at 1 week (*E*), 2 weeks (*F*), and 3 weeks (*G*) PTI. In $^{tam}Kif3a^{+/-}$ (*left*), axonemes (*red*) emanate from the GFP-CENT2-labeled PTZ and extend into the OS. $^{tam}Kif3a^{-/-}$ axonemes are shortened as early as 1 week PTI (*E*, *right*) and progress at 2 weeks PTI (*F*, *right*), and by 3 weeks PTI (*G*, *right*), most axonemes are severely shortened and disorganized as OSs have disintegrated. *H*, decrease of axoneme length in $^{tam}Kif3a^{+/-}$;*Cetn2*$^{+}$ and $^{tam}Kif3a^{-/-}$;*Cetn2*$^{+}$ photoreceptors (50 photoreceptors each) at 1, 2, and 3 weeks PTI. *, $p < 0.01$. *Error bars* indicate mean ± S.E. *I* and *J*, $^{tam}Kif3a^{+/-}$ and $^{tam}Kif3a^{-/-}$ axonemes labeled with anti-acetylated α-tubulin (*Ac-tub*) antibody (*red*) at 1 week (*I*) and 2 weeks (*J*) PTI. Relative to $^{tam}Kif3a^{+/-}$ photoreceptors (*left*), Ac-tub-labeled axonemes (*red*) of $^{tam}Kif3a^{-/-}$ photoreceptor OS are shortened and disorganized. Tubulin apparently is retained in the IS at 1 week PTI (*I*, *right*). At 2 weeks PTI, tubulin immunolabeling is much reduced in $^{tam}Kif3a^{-/-}$ photoreceptors (*J*, *right*).

was undetectable by immunohistochemistry in the ONL and inner segments 1 week post-tamoxifen induction (Fig. 4, *E–G*, *right*). Trafficking of rhodopsin and other OS components proceeded normally in the absence of Kif3A for about 3 weeks post-tamoxifen induction (Fig. 4, *H–J*, and Fig. 6). In the adult mouse, rod and cone outer segments are completely replaced every 10 days, requiring resynthesis of 80 OS disks every days (57); therefore 3 weeks are sufficient to replace outer segments twice. Outer segment proteins continued to travel even after onset of OS degeneration (Figs. 4 and 6), a finding consistent

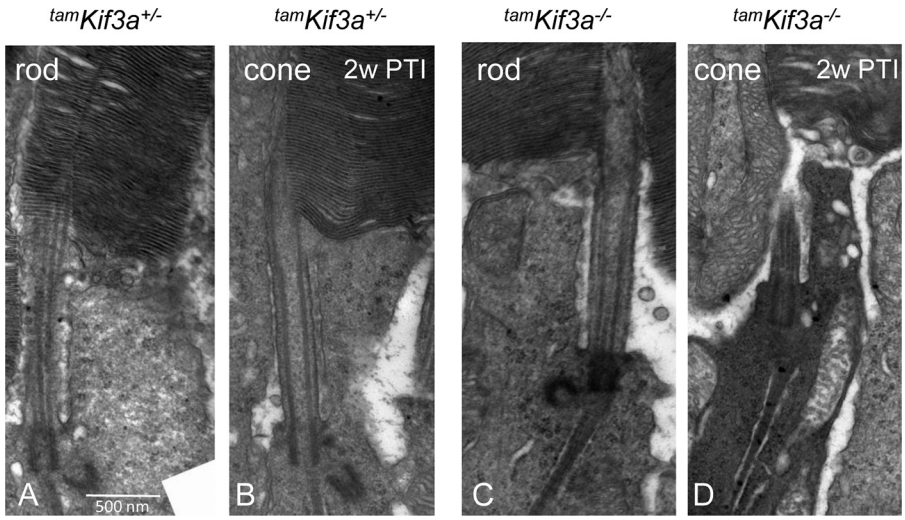

FIGURE 10. **Ultrastructure of $^{tam}Kif3a^{+/-}$ and $^{tam}Kif3a^{-/-}$ photoreceptors.** *A–D*, at 2 weeks PTI (*2w PTI*), $^{tam}Kif3a^{+/-}$ rods and cones have normal photoreceptor OS structures (*A* and *B*). $^{tam}Kif3^{-/-}$ rod (*C*) and cone (*D*) have intact PTZs, but $^{tam}Kif3a^{-/-}$ cones show cytoplasmic condensation of an early stage leading to cell death.

with our previous study in which transgenic expression of *iCre75* caused rod and ROS degeneration, but did not interfere with rhodopsin trafficking (32).

Surprisingly, cone pigment trafficking in $^{tam}Kif3a^{-/-}$ cones progressed normally as well (Fig. 4, *K–P*, *right*), although cone pigment mislocalization and degeneration was observed earlier than in rods, about 2 weeks after the first injection of tamoxifen (Fig. 4, *L–O*, *right*). COS renewal proceeded normally in the absence of KIF3A. This contrasts with our previous study (32) in which transgenic *Cre* expression in cones under control of the human red/green promoter resulted in the early mislocalization of cone pigments and absence of OS components in $^{tam}Kif3a^{-/-}$ COS. The discrepancy may be explained by differences in *Cre* drivers (transgenic *versus* tamoxifen-induced depletion), onset of *Cre* expression (early expression during cone development *versus* adult), and varying *Cre* expression levels. Tamoxifen-induced deletion of IFT88 did not affect OS protein trafficking as long as an OS and axoneme existed (Fig. 8*C*).

We were intrigued by the different rates of outer segment degeneration in rods *versus* cones and asked whether this may be caused by differences in outer segment structure, disc membrane organization, or intrinsic properties of visual pigment. Ectopic expression of S-opsin in $Rho^{-/-}$ rods restored outer segments and their ability to respond to light (42). S-opsin expressed in $^{tam}Kif3^{-/-}$ rods under rhodopsin knock-out or heterozygous background trafficked normally to the OSs at 2 and 3 weeks PTI, nearly indistinguishable from controls (Fig. 7, D and F, *right*). In contrast, native ML-opsin in cones still mistrafficked in the S-opsin expressed in $^{tam}Kif3^{-/-}$ mice at 2 week PTI, and COS fell apart at 3 weeks PTI (Fig. 7, *C–E*, *right*). These experiments demonstrate that S-opsin expressed in rods follows the mistrafficking and degeneration pattern observed with rhodopsin in $^{tam}Kif3a$ rod OS.

The main effect of KIF3A deletion in the adult mouse retina was gradual shortening of the axoneme, as documented by labeling with antibodies directed against RP1 and Ac-tubulin (Fig. 9, *D–F*, *I*, and *J*). An axoneme extends from the basal body, through the PTZ into the OS to about half-length in the rod and to the cone tip in *Xenopus* (61). The precise axoneme extension in much smaller mouse rods and cones is unknown. Ciliary axonemes require microtubule plus-end tracking and continuous co-polymerization of α- and β-tubulin subunits at their distal tips, and this process is highly dependent on a kinesin-2-mediated IFT pathway (62, 63). Our results are consistent with a role of KIF3 in axonemal maintenance, in which KIF3 powers IFT trains carrying axonemal tubulin subunits or other ciliary membrane building blocks. Cargo transports to the axoneme distal tip where axoneme assembly and turnover occur. Interruption of KIF3-based IFT is sufficient to deteriorate the axoneme distally, with progressive shortening of the OS and eventual photoreceptor degeneration.

If rhodopsin trafficking through the PTZ is independent of IFT, what trafficking routes are available for rhodopsin? Because of continuous OS turnover, rod trafficking requires a flow of ~70 rhodopsin molecules per second to be advanced through the PTZ. In *Xenopus*, an animal with very large photoreceptors, the flow increases to several hundred rhodopsins/second (64). Alternative trafficking pathways have been proposed in which rhodopsin-containing vesicles stream toward the OS, without motor activity, inside the axonemal shaft to eventually expand into large disk membranes at the proximal OS (33, 65). Clearly, water-insoluble rhodopsin requires membrane support for trafficking, either within freely floating vesicles or in membrane-embedded cargo. By immuno-EM, rhodopsin has been observed at the PTZ plasma membrane, supporting lateral membrane diffusion. As the nature of cargo (*i.e.* carrier vesicle constituents) is undefined, our knowledge is limited and incomplete.

In summary, *KIF3a* conditional knock-out in mouse retina progenitors prevents rod/cone axoneme formation and OS morphogenesis. Tamoxifen-induced KIF3A deletion in the adult mouse impedes photoreceptor axoneme maintenance, leading to progressive OS shortening from distal-to-proximal with subsequent photoreceptor degeneration. These experiments demonstrate collectively that IFT powered by heterotri-

meric kinesin-2 is critical for axoneme initiation/maintenance, and consequently, photoreceptor OS structure. Further, kinesin-2 molecular motors and IFT88 are nonessential for ciliary trafficking of visual pigment and accessory OS proteins.

Acknowledgments—We thank Kevin Rapp for assistance in TEM experiments. The IFT88 conditional allele was provided by the National Institutes of Health supported Heptorenal Fibrocystic Disease Core Center (HRFDCC, P30 DK074038, B. Yoder).

REFERENCES

1. Sorokin, S. P. (1968) Reconstructions of centriole formation and ciliogenesis in mammalian lungs. *J. Cell Sci.* **3,** 207–230
2. Satir, P., Pedersen, L. B., and Christensen, S. T. (2010) The primary cilium at a glance. *J. Cell Sci.* **123,** 499–503
3. Goetz, S. C., and Anderson, K. V. (2010) The primary cilium: a signalling centre during vertebrate development. *Nat. Rev. Genet.* **11,** 331–344
4. Satir, P., and Christensen, S. T. (2007) Overview of structure and function of mammalian cilia. *Annu. Rev. Physiol.* **69,** 377–400
5. Scholey, J. M. (2013) Cilium assembly: delivery of tubulin by kinesin-2-powered trains. *Curr. Biol.* **23,** R956–R959
6. Praetorius, H. A., and Spring, K. R. (2003) The renal cell primary cilium functions as a flow sensor. *Curr. Opin. Nephrol. Hypertens.* **12,** 517–520
7. Kaupp, U. B. (2010) Olfactory signalling in vertebrates and insects: differences and commonalities. *Nat. Rev. Neurosci.* **11,** 188–200
8. Lamb, T. D., and Pugh, E. N., Jr. (2006) Phototransduction, dark adaptation, and rhodopsin regeneration the proctor lecture. *Invest. Ophthalmol. Vis. Sci.* **47,** 5137–5152
9. Insinna, C., and Besharse, J. C. (2008) Intraflagellar transport and the sensory outer segment of vertebrate photoreceptors. *Dev. Dyn.* **237,** 1982–1992
10. Rosenbaum, J. L., and Witman, G. B. (2002) Intraflagellar transport. *Nat. Rev. Mol. Cell Biol.* **3,** 813–825
11. Scholey, J. M. (2008) Intraflagellar transport motors in cilia: moving along the cell's antenna. *J. Cell Biol.* **180,** 23–29
12. Scholey, J. M. (2013) Kinesin-2: a family of heterotrimeric and homodimeric motors with diverse intracellular transport functions. *Annu. Rev. Cell Dev. Biol.* **29,** 443–469
13. Fliegauf, M., Benzing, T., and Omran, H. (2007) When cilia go bad: cilia defects and ciliopathies. *Nat. Rev. Mol. Cell Biol.* **8,** 880–893
14. Pazour, G. J., Dickert, B. L., Vucica, Y., Seeley, E. S., Rosenbaum, J. L., Witman, G. B., and Cole, D. G. (2000) *Chlamydomonas IFT88* and its mouse homologue, polycystic kidney disease gene *Tg737*, are required for assembly of cilia and flagella. *J. Cell Biol.* **151,** 709–718
15. Sukumaran, S., and Perkins, B. D. (2009) Early defects in photoreceptor outer segment morphogenesis in zebrafish *ift57*, *ift88*, and *ift172* intraflagellar transport mutants. *Vision Res.* **49,** 479–489
16. Murcia, N. S., Richards, W. G., Yoder, B. K., Mucenski, M. L., Dunlap, J. R., and Woychik, R. P. (2000) The *Oak Ridge Polycystic Kidney* (*orpk*) disease gene is required for left-right axis determination. *Development* **127,** 2347–2355
17. Moyer, J. H., Lee-Tischler, M. J., Kwon, H. Y., Schrick, J. J., Avner, E. D., Sweeney, W. E., Godfrey, V. L., Cacheiro, N. L., Wilkinson, J. E., and Woychik, R. P. (1994) Candidate gene associated with a mutation causing recessive polycystic kidney disease in mice. *Science* **264,** 1329–1333
18. Pazour, G. J., Baker, S. A., Deane, J. A., Cole, D. G., Dickert, B. L., Rosenbaum, J. L., Witman, G. B., and Besharse, J. C. (2002) The intraflagellar transport protein, IFT88, is essential for vertebrate photoreceptor assembly and maintenance. *J. Cell Biol.* **157,** 103–113
19. McIntyre, J. C., Davis, E. E., Joiner, A., Williams, C. L., Tsai, I. C., Jenkins, P. M., McEwen, D. P., Zhang, L., Escobado, J., Thomas, S., Szymanska, K., Johnson, C. A., Beales, P. L., Green, E. D., Mullikin, J. C., NISC Comparative Sequencing Program, Sabo, A., Muzny, D. M., Gibbs, R. A., Attié-Bitach, T., Yoder, B. K., Reed, R. R., Katsanis, N., and Martens, J. R. (2012) Gene therapy rescues cilia defects and restores olfactory function in a mammalian ciliopathy model. *Nat. Med.* **18,** 1423–1428
20. Davenport, J. R., Watts, A. J., Roper, V. C., Croyle, M. J., van Groen, T., Wyss, J. M., Nagy, T. R., Kesterson, R. A., and Yoder, B. K. (2007) Disruption of intraflagellar transport in adult mice leads to obesity and slow-onset cystic kidney disease. *Curr. Biol.* **17,** 1586–1594
21. Bhowmick, R., Li, M., Sun, J., Baker, S. A., Insinna, C., and Besharse, J. C. (2009) Photoreceptor IFT complexes containing chaperones, guanylyl cyclase 1 and rhodopsin. *Traffic* **10,** 648–663
22. Cole, D. G., Cande, W. Z., Baskin, R. J., Skoufias, D. A., Hogan, C. J., and Scholey, J. M. (1992) Isolation of a sea urchin egg kinesin-related protein using peptide antibodies. *J. Cell Sci.* **101,** 291–301
23. Cole, D. G., Chinn, S. W., Wedaman, K. P., Hall, K., Vuong, T., and Scholey, J. M. (1993) Novel heterotrimeric kinesin-related protein purified from sea urchin eggs. *Nature* **366,** 268–270
24. Cole, D. G., Diener, D. R., Himelblau, A. L., Beech, P. L., Fuster, J. C., and Rosenbaum, J. L. (1998) *Chlamydomonas* kinesin-II-dependent intraflagellar transport (IFT): IFT particles contain proteins required for ciliary assembly in *Caenorhabditis elegans* sensory neurons. *J. Cell Biol.* **141,** 993–1008
25. Kozminski, K. G., Forscher, P., and Rosenbaum, J. L. (1998) Three flagellar motilities in *Chlamydomonas* unrelated to flagellar beating. Video supplement. *Cell Motil. Cytoskeleton* **39,** 347–348
26. Signor, D., Wedaman, K. P., Rose, L. S., and Scholey, J. M. (1999) Two heteromeric kinesin complexes in chemosensory neurons and sensory cilia of *Caenorhabditis elegans*. *Mol. Biol. Cell* **10,** 345–360
27. Wong-Riley, M. T., and Besharse, J. C. (2012) The kinesin superfamily protein KIF17: one protein with many functions. *Biomol. Concepts* **3,** 267–282
28. Bader, J. R., Kusik, B. W., and Besharse, J. C. (2012) Analysis of KIF17 distal tip trafficking in zebrafish cone photoreceptors. *Vision Res.* **75,** 37–43
29. Marszalek, J. R., Liu, X., Roberts, E. A., Chui, D., Marth, J. D., Williams, D. S., and Goldstein, L. S. (2000) Genetic evidence for selective transport of opsin and arrestin by kinesin-II in mammalian photoreceptors. *Cell* **102,** 175–187
30. Jimeno, D., Feiner, L., Lillo, C., Teofilo, K., Goldstein, L. S., Pierce, E. A., and Williams, D. S. (2006) Analysis of kinesin-2 function in photoreceptor cells using synchronous *Cre*-loxP knockout of *Kif3a* with *RHO-Cre*. *Invest. Ophthalmol. Vis. Sci.* **47,** 5039–5046
31. Lin, F., Hiesberger, T., Cordes, K., Sinclair, A. M., Goldstein, L. S., Somlo, S., and Igarashi, P. (2003) Kidney-specific inactivation of the KIF3A subunit of kinesin-II inhibits renal ciliogenesis and produces polycystic kidney disease. *Proc. Natl. Acad. Sci. U.S.A.* **100,** 5286–5291
32. Avasthi, P., Watt, C. B., Williams, D. S., Le, Y. Z., Li, S., Chen, C. K., Marc, R. E., Frederick, J. M., and Baehr, W. (2009) Trafficking of membrane proteins to cone but not rod outer segments is dependent on heterotrimeric kinesin-II. *J. Neurosci.* **29,** 14287–14298
33. Chuang, J. Z., Zhao, Y., and Sung, C. H. (2007) SARA-regulated vesicular targeting underlies formation of the light-sensing organelle in mammalian rods. *Cell* **130,** 535–547
34. Gilliam, J. C., Chang, J. T., Sandoval, I. M., Zhang, Y., Li, T., Pittler, S. J., Chiu, W., and Wensel, T. G. (2012) Three-dimensional architecture of the rod sensory cilium and its disruption in retinal neurodegeneration. *Cell* **151,** 1029–1041
35. Scholey, J. M. (2012) Kinesin-2 motors transport IFT-particles, dyneins and tubulin subunits to the tips of *Caenorhabditis elegans* sensory cilia: relevance to vision research? *Vision Res* **75,** 44–52
36. Haycraft, C. J., Zhang, Q., Song, B., Jackson, W. S., Detloff, P. J., Serra, R., and Yoder, B. K. (2007) Intraflagellar transport is essential for endochondral bone formation. *Development* **134,** 307–316
37. Furuta, Y., Lagutin, O., Hogan, B. L., and Oliver, G. C. (2000) Retina- and ventral forebrain-specific Cre recombinase activity in transgenic mice. *Genesis* **26,** 130–132
38. Hayashi, S., and McMahon, A. P. (2002) Efficient recombination in diverse tissues by a tamoxifen-inducible form of Cre: a tool for temporally regulated gene activation/inactivation in the mouse. *Dev. Biol.* **244,** 305–318
39. Li, S., Chen, D., Sauvé, Y., McCandless, J., Chen, Y. J., and Chen, C.-K. (2005) Rhodopsi-iCre transgenic mouse line for Cre-mediated rod-specific gene targeting. *Genesis* **41,** 73–80

40. Lakso, M., Pichel, J. G., Gorman, J. R., Sauer, B., Okamoto, Y., Lee, E., Alt, F. W., and Westphal, H. (1996) Efficient *in vivo* manipulation of mouse genomic sequences at the zygote stage. *Proc. Natl. Acad. Sci. U.S.A.* **93,** 5860–5865
41. Lem, J., Krasnoperova, N. V., Calvert, P. D., Kosaras, B., Cameron, D. A., Nicolò, M., Makino, C. L., and Sidman, R. L. (1999) Morphological, physiological, and biochemical changes in rhodopsin knockout mice. *Proc. Natl. Acad. Sci. U.S.A.* **96,** 736–741
42. Shi, G., Yau, K. W., Chen, J., and Kefalov, V. J. (2007) Signaling properties of a short-wave cone visual pigment and its role in phototransduction. *J. Neurosci.* **27,** 10084–10093
43. Higginbotham, H., Bielas, S., Tanaka, T., and Gleeson, J. G. (2004) Transgenic mouse line with green-fluorescent protein-labeled Centrin 2 allows visualization of the centrosome in living cells. *Transgenic. Res.* **13,** 155–164
44. Baehr, W., Karan, S., Maeda, T., Luo, D. G., Li, S., Bronson, J. D., Watt, C. B., Yau, K. W., Frederick, J. M., and Palczewski, K. (2007) The function of guanylate cyclase 1 and guanylate cyclase 2 in rod and cone photoreceptors. *J. Biol. Chem.* **282,** 8837–8847
45. Jiang, L., Zhang, H., Dizhoor, A. M., Boye, S. E., Hauswirth, W. W., Frederick, J. M., and Baehr, W. (2011) Long-term RNA interference gene therapy in a dominant retinitis pigmentosa mouse model. *Proc. Natl. Acad. Sci. U.S.A.* **108,** 18476–18481
46. Jones, B. W., Kondo, M., Terasaki, H., Watt, C. B., Rapp, K., Anderson, J., Lin, Y., Shaw, M. V., Yang, J. H., and Marc, R. E. (2011) Retinal remodeling in the Tg P347L rabbit, a large-eye model of retinal degeneration. *J. Comp. Neurol.* **519,** 2713–2733
47. Zhang, J., Fuhrmann, S., and Vetter, M. L. (2008) A nonautonomous role for retinal frizzled-5 in regulating hyaloid vitreous vasculature development. *Invest. Ophthalmol. Vis. Sci.* **49,** 5561–5567
48. Giessl, A., Trojan, P., Rausch, S., Pulvermüller, A., and Wolfrum, U. (2006) Centrins, gatekeepers for the light-dependent translocation of transducin through the photoreceptor cell connecting cilium. *Vision Res.* **46,** 4502–4509
49. Ying, G., Avasthi, P., Irwin, M., Gerstner, C. D., Frederick, J. M., Lucero, M. T., and Baehr, W. (2014) Centrin 2 is required for mouse olfactory ciliary trafficking and development of ependymal cilia planar polarity. *J. Neurosci.* **34,** 6377–6388
50. Williams, C. L., Li, C., Kida, K., Inglis, P. N., Mohan, S., Semenec, L., Bialas, N. J., Stupay, R. M., Chen, N., Blacque, O. E., Yoder, B. K., and Leroux, M. R. (2011) MKS and NPHP modules cooperate to establish basal body/transition zone membrane associations and ciliary gate function during ciliogenesis. *J. Cell Biol.* **192,** 1023–1041
51. Kodani, A., Salomé Sirerol-Piquer, M., Seol, A., Garcia-Verdugo, J. M., and Reiter, J. F. (2013) Kif3a interacts with Dynactin subunit $p150^{Glued}$ to organize centriole subdistal appendages. *EMBO J.* **32,** 597–607
52. Qin, H., Rosenbaum, J. L., and Barr, M. M. (2001) An autosomal recessive polycystic kidney disease gene homolog is involved in intraflagellar transport in *C. elegans* ciliated sensory neurons. *Curr. Biol.* **11,** 457–461
53. Haycraft, C. J., Swoboda, P., Taulman, P. D., Thomas, J. H., and Yoder, B. K. (2001) The *C. elegans* homolog of the murine cystic kidney disease gene *Tg737* functions in a ciliogenic pathway and is disrupted in *osm-5* mutant worms. *Development* **128,** 1493–1505
54. Neugebauer, J. M., Amack, J. D., Peterson, A. G., Bisgrove, B. W., and Yost, H. J. (2009) FGF signalling during embryo development regulates cilia length in diverse epithelia. *Nature* **458,** 651–654
55. Onuchic, L. F., Schrick, J. J., Ma, J., Hudson, T., Guay-Woodford, L. M., Zerres, K., Woychik, R. P., and Reeders, S. T. (1995) Sequence analysis of the human hTg737 gene and its polymorphic sites in patients with autosomal recessive polycystic kidney disease. *Mamm. Genome.* **6,** 805–808
56. Trivedi, D., Colin, E., Louie, C. M., and Williams, D. S. (2012) Live-cell imaging evidence for the ciliary transport of rod photoreceptor opsin by heterotrimeric kinesin-2. *J. Neurosci.* **32,** 10587–10593
57. Young, R. W. (1976) Visual cells and the concept of renewal. *Invest Ophthalmol. Vis. Sci.* **15,** 700–725
58. Liu, Q., Lyubarsky, A., Skalet, J. H., Pugh, E. N., Jr., and Pierce, E. A. (2003) RP1 is required for the correct stacking of outer segment discs. *Invest. Ophthalmol. Vis. Sci.* **44,** 4171–4183
59. Yamashita, T., Liu, J., Gao, J., LeNoue, S., Wang, C., Kaminoh, J., Bowne, S. J., Sullivan, L. S., Daiger, S. P., Zhang, K., Fitzgerald, M. E., Kefalov, V. J., and Zuo, J. (2009) Essential and synergistic roles of RP1 and RP1L1 in rod photoreceptor axoneme and retinitis pigmentosa. *J. Neurosci.* **29,** 9748–9760
60. Olney, J. W. (1968) An electron microscopic study of synapse formation, receptor outer segment development, and other aspects of developing mouse retina. *Invest. Ophthalmol.* **7,** 250–268
61. Eckmiller, M. S., and Toman, A. (1998) Association of kinesin with microtubules in diverse cytoskeletal systems in the outer segments of rods and cones. *Acta Anat. (Basel)* **162,** 133–141
62. Akhmanova, A., and Steinmetz, M. O. (2008) Tracking the ends: a dynamic protein network controls the fate of microtubule tips. *Nat. Rev. Mol. Cell Biol.* **9,** 309–322
63. Conde, C., and Cáceres, A. (2009) Microtubule assembly, organization and dynamics in axons and dendrites. *Nat. Rev. Neurosci.* **10,** 319–332
64. Pearring, J. N., Salinas, R. Y., Baker, S. A., and Arshavsky, V. Y. (2013) Protein sorting, targeting and trafficking in photoreceptor cells. *Prog. Retin. Eye. Res* **36,** 24–51
65. Chuang, J. Z., Hsu, Y. C., and Sung, C. H. (2015) Ultrastructural visualization of trans-ciliary rhodopsin cargoes in mammalian rods. *Cilia* **4,** 4